Journal of Mineralogical and Petrological Sciences, Volume 110, page 166–178, 2015

Geochemical behavior of zirconium during Cl-rich fluid or melt infiltration under upper amphibolite facies metamorphism — A case study from Brattnipene, Sør Rondane Mountains, East Antarctica

Fumiko HIGASHINO[*,#], Tetsuo KAWAKAMI[*], Noriyoshi TSUCHIYA[**], M. SATISH-KUMAR[***], Masahiro ISHIKAWA[†], Geoffrey H. GRANTHAM[‡], Shuhei SAKATA[*], Kentaro HATTORI[*] and Takafumi HIRATA[*]

[*]*Department of Geology and Mineralogy, Graduate School of Science, Kyoto University, Kyoto 606-8502, Japan*
[**]*Graduate School of Environmental Studies, Tohoku University, Sendai 980-9570, Japan*
[***]*Department of Geology, Faculty of Science, Niigata University, Niigata 950-2181, Japan*
[†]*Graduate School of Environment and Information Sciences, Yokohama National University, Yokohama 240-8501, Japan*
[‡]*Department of Geology, University of Johannesburg, South Africa*

The appropriateness of Zr as an 'immobile element' during garnet-hornblende (Grt-Hbl) vein formation potentially caused by the Cl-rich fluid or melt infiltration under upper amphibolite facies condition is examined. The sample used is a Grt-Hbl vein from Brattnipene, Sør Rondane Mountains, East Antarctica that discordantly cuts the gneissose structure of the mafic gneiss.

Modal analysis of the wall rock minerals combined with the quantitative determination of their Zr contents reveals that most of the whole-rock Zr resides in zircon whereas ~ 5% is hosted in garnet and hornblende. The Zr concentration of garnet and hornblende is constant irrespective of the distance from the vein. Zircon shows no resorption or overgrowth microstructures. Moreover, the grain size, chemical zoning (CL, Th/U ratio and REE pattern) and rim ages of zircon are also similar irrespective of the distance from the vein. LA-ICPMS U-Pb dating of zircon rims does not give younger ages than the granulite facies metamorphism reported by previous studies. All of these detailed observations on zircon support that zircon is little dissolved or overgrown, and that Zr is not added nor lost during the Grt-Hbl vein formation. Therefore, Zr can be described as an appropriate 'immobile element' during the Grt-Hbl vein formation. Detailed microstructural observation of zircon is thus useful in evaluating the appropriateness of Zr as an immobile element.

Keywords: Chlorine, Immobile element, Zirconium, REE pattern, U-Pb dating

INTRODUCTINON

In order to estimate a relative mass addition/loss during metasomatism and weathering, methods such as isocon analysis (e.g., Grant, 1986) and calculation of the fractional mass change (Ague, 2003) are proposed. In these methods, at least one 'immobile element' must be determined as a reference element (e.g., Olsen and Grant, 1991; Whitbread and Moore, 2004; Mori et al., 2007). The 'immobile element' should be carefully selected based on supporting evidence and not simply assumed, because whether and how much of other elements are added or lost greatly depends on this selection. In many previous studies, elemental immobility was established by using a bootstrap estimation (Ague and Van Haren, 1996) or by using petrological and mineralogical microstructures as evidence (e.g., Gao et al., 2007; Mori et al., 2007). As a result, Zr, Nb, Y, Hf, and Th are often described as immobile elements (Gao et al., 2007). These elements could be stored in minerals difficult to be dissolved by hydrothermal fluids in the case of high-grade metamorphic rocks.

Most of the whole-rock Zr in crustal rocks is hosted in zircon (Hermann, 2002; Dill, 2010). Zircon is less susceptible to secondary alteration in the presence of fluids

doi:10.2465/jmps.150220
F. Higashino, fumitan@kueps.kyoto-u.ac.jp Corresponding author
[#] JSPS Research Fellow

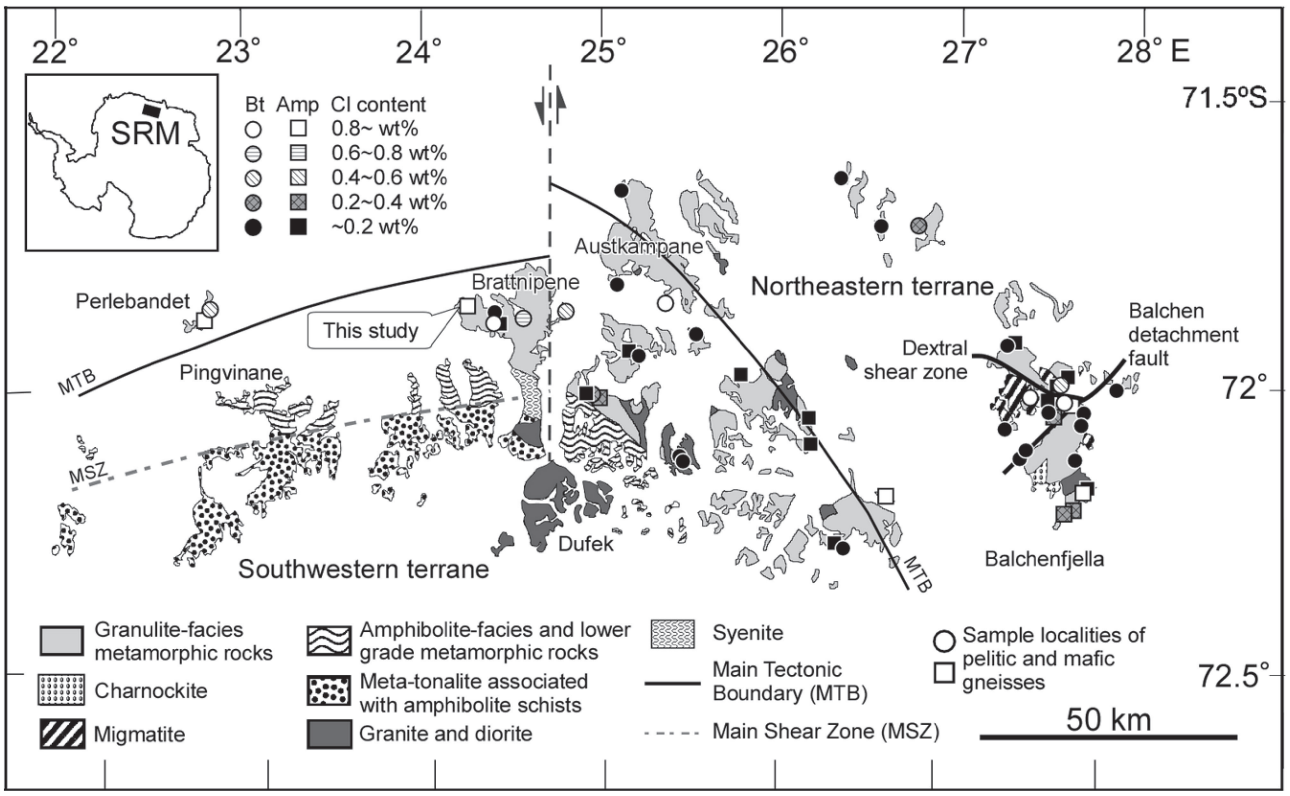

Figure 1. Simplified geological map of the Sør Rondane Mountains (after Shiraishi et al., 2008; Osanai et al., 2013; Toyoshima et al., 2013; Ishikawa et al., 2013; Higashino et al., 2013b). Detailed geological and tectonic explanation can be found in Osanai et al. (2013) and Toyoshima et al. (2013).

compared to other rock-forming minerals (Rubin et al., 1993; Ayers and Watson, 1991; Taylor et al. 2014). This would be the reason Zr is often selected as being an 'immobile element'. However, an experimental study by Harlov and Dunkley (2011) concluded that zircon can be dissolved in fluids depending on fluid compositions and pressure-temperature (*P-T*) conditions. Zircon can also be altered by Cl-rich brines during high-*T* metamorphism (Dunkley, 2010). Therefore, in mass transfer analysis, it is important to select appropriate 'immobile elements' for each sample, taking into account the microstructures of rock-forming minerals and petrographic observations (Olsen and Grant, 1991).

In Brattnipene, central Sør Rondane Mountains, East Antarctica, ~ 1 cm-thick garnet-hornblende (Grt-Hbl) veins discordantly cut the gneissose structure of the wall rock (Higashino et al., 2013a). Infiltration of Cl-rich fluid or melt is inferred in this sample, because major and trace element compositions of minerals in the vein and the wall rock, including Cl content in biotite and hornblende, systematically change with distance from the vein center (Higashino et al., 2013a). Using this sample, this study firstly shows that zircon hosts most of the whole-rock Zr. Secondly, we discuss the appropriateness of Zr as an 'immobile element' in the wall rock, based on the detailed microstructural observations, chemistry of Zr-hosting minerals, and the U-Pb ages of zircon. Mineral abbreviations are after Kretz (1983).

GEOLOGICAL SETTING

The Sør Rondane Mountains (SRM; 22°-28°E, 71.5°-72.5°S), eastern Dronning Maud Land, East Antarctica are dominated by granulite facies metamorphic rocks and granitoids (Shiraishi et al., 1991; Asami et al., 1992). The SRM is thought to be a part of the collision zone between East and West Gondwana during the East African-Antarctic Orogen (Jacobs and Thomas, 2004) and is also interpreted to be in the hanging wall of a mega-nappe complex involving continental collision between northern and southern Gondwana (Grantham et al., 2013) during the Kuunga Orogeny of Meert (2003). The SRM have been divided into the NE terrane and the SW terrane by a mylonite zone named the Main Tectonic Boundary that dips gently to the north and northeast (Osanai et al., 2013) (Fig. 1). The NE terrane rocks record clockwise *P-T* paths, whereas the SW terrane rocks record counter-clockwise *P-T* paths (Osanai et al., 2013).

For further detailed geological and tectonic explanation, see Osanai et al. (2013) and Toyoshima et al. (2013).

In northern Brattnipene, which belongs to the SW terrane, peak metamorphic *P–T* conditions are estimated to be ~ 800 °C and ~ 0.70–0.85 GPa (Shiraishi and Kojima, 1987; Adachi et al., 2013a), and a counter-clockwise *P–T* path is proposed (Adachi et al., 2013a). Previous SHRIMP U-Pb zircon dating of an enderbitic orthogneiss from northwestern Brattnipene gave an igneous protolith age of 951 ± 17 Ma, and a granulite-grade metamorphic age of 602 ± 15 Ma (Shiraishi et al., 2008). From northwestern Brattnipene, SHRIMP U-Pb zircon ages of an orthopyroxene-clinopyroxene (Opx-Cpx) felsic gneiss and an undeformed pegmatite vein which intrudes the Opx-Cpx felsic gneiss are also reported (Adachi et al., 2013b). The weighted mean $^{206}Pb/^{238}U$ age of unzoned, bright-cathodoluminescence (bright-CL) zircon domains from the Opx-Cpx felsic gneiss gave 627 ± 15 Ma, and was interpreted as the timing of metamorphism (Adachi et al., 2013b). Timing of the pegmatite intrusion, on the other hand, was dated to be 546 ± 4 Ma (weighted mean $^{207}Pb/^{206}Pb$ age; Adachi et al., 2013b).

The Cl-rich mineral distribution can be traced for ~ 200 km from the east to the west of the SRM (Higashino et al., 2013b) (Fig. 1). Higashino et al. (2013b) reported that the Cl-rich fluid or melt activity affected biotite and apatite in pelitic gneisses, during early retrograde metamorphism near the peak metamorphic *P–T* condition of ~ 800 °C and ~ 0.8 GPa at Balchenfjella, eastern SRM. Magmatic hornblende has also been reported to show relatively high halogen contents in some granitoids in the SRM. Li et al. (2007) reported hornblende with 1.15–1.23 wt% F and 0.28–0.32 wt% Cl from the Dufek granite, and hornblende with 0.25–0.43 wt% F and 0.31–0.41 wt% Cl from the Pingvinane granite.

ANALYTICAL METHODS

Quantitative analysis, and X-ray elemental mapping of minerals, and CL imaging of zircon were performed using a JEOL JXA-8105 superprobe equipped with Hamamatsu Photonics high voltage power supply C9525 and photon counting unit C9744 at Kyoto University. Analytical conditions for quantitative analyses were an accelerating voltage of 15.0 kV and a beam current of 10 nA with a probe diameter of 3 μm. Counting time for the peak and backgrounds were 30 s and 15 s for Cl, 60 s and 30 s for F, and 10 s and 5 s for other elements, respectively. Natural and synthetic minerals were used as standards and a ZAF correction method was applied. Analytical conditions for X-ray elemental mapping were an accelerating voltage of 15.0 kV and a probe current of 60 nA with a focused beam to defocused beam having a diameter of 10 μm.

In situ U-Pb zircon dating on thin section samples by a laser ablation inductively coupled plasma mass spectrometry (LA-ICPMS) was carried out using a Nu Plasma II HR-MC-ICPMS coupled to a NWR Femto femtosecond laser-ablation system (Hirata and Nesbitt, 1995; Iizuka and Hirata, 2004). Backscattered electron (BSE) and CL images were obtained prior to the analyses to identify spot positions, overlapping multiple growth zones, grain edges, cracks or damaged zircon grains. Data were processed and plotted using Isoplot 4.13 (Ludwig, 2008). In situ LA-ICPMS analyses of rare earth elements (REE) and trace element concentrations of zircon, garnet, hornblende, orthopyroxene, biotite, plagioclase and apatite were performed by an iCAP-Qc quadrupole-based ICPMS coupled with a NWR Femto femtosecond laser-ablation system or a NWR-193 ArF Excimer laser-ablation system (Hirata and Kon, 2008; Sakata et al., 2014). Analytical conditions for the LA-ICPMS analyses are summarized in supplementary Tables S1 and S2 (Tables S1 and S2 are available online from http://doi.org/10.2465/jmps.150220.). All of the above analyses were done at Department of Geology and Mineralogy, Kyoto University.

Concentration of whole-rock Zr was determined using solution ICPMS at Tohoku University. Rock powders were prepared in a tungsten-carbide mill at Kyoto University and samples were prepared by acid digestion after alkali fusion. Indium was used for an internal standard (Yamasaki, 1996; Yamasaki et al., 2013).

SAMPLE LOCALITY

At Brattnipene, mafic lithologies are commonly intercalated with pelitic lithologies, intermediate hornblende gneisses, marble, and locally contain peridotite and pyroxenite lenses. The gneissose structure of the host gneiss is discordantly cut by a network of cm-thick Grt-Hbl veins. The vein consists of garnet and hornblende that are coarser-grained than the host mafic gneiss (Fig. 2a). Sample TK2009121002C, used in this study contains a Grt-Hbl vein which cuts mafic gneisses (Grt-Opx-Hbl gneiss) and was collected from a layered sequence of mafic gneisses in northwestern Brattnipene during 51st Japan Antarctic Research Expedition (JARE51) (Tsuchiya et al., 2012) (Fig. 1). The sample locality of TK2009121002C is ~ 700 m SE from that of the enderbitic orthogneiss whose metamorphic age was estimated to be 602 ± 15 Ma (Shiraishi et al., 2008), and ~ 190 m SE from that of the Opx-Cpx felsic gneiss whose metamorphic age

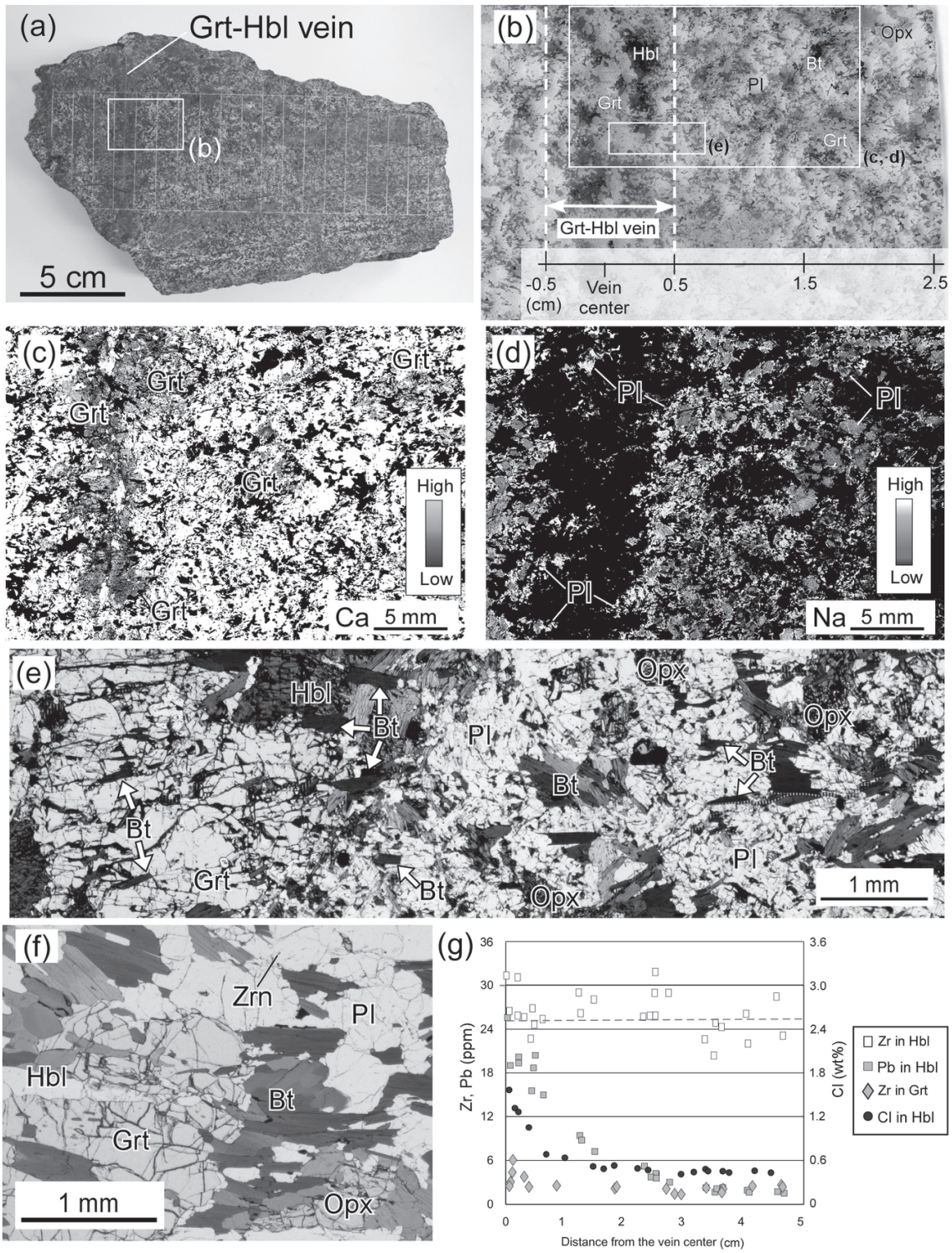

Figure 2. (a) Slab photo of the Grt-Opx-Hbl gneiss (sample TK2009121002C) used in this study. About 1 cm-thick Grt-Hbl vein discordantly cuts the gneissose structure. (b) Photo of a thin section of boxed area in (a). A Grt-Hbl vein consists of coarse-grained garnet and hornblende. Plane polarized light (PPL). (c) X-ray elemental map of Ca of boxed area in (b). The Ca-poor domain of garnet is abundant near the vein. (d) X-ray elemental map of Na of boxed area in (b). The Na-richer rim of plagioclase gets thinner with distance from the vein center. (e) Photomicrograph of boxed area in (b), which corresponds to the area from the vein center to the wall rock. Orthopyroxene is absent in the vein. Note the continuous gneissose structure preserved as biotite arrangements included in the vein-forming garnet. PPL. (f) Photomicrograph of the area ~ 3 cm away from the vein center. Garnet and orthopyroxene is present. Quartz is rarely present. PPL. (g) Variation in hornblende and garnet composition as a function of distance from the Grt-Hbl vein center. Chlorine and Pb concentration of hornblende decreases with distance from the vein center. Dotted line shows an approximate line defined for Zr concentration of hornblende.

was estimated to be 627 ± 15 Ma (Adachi et al., 2013b).

SAMPLE DESCRIPTION OF THE GRT-OPX-HBL GNEISS WITH A GRT-HBL VEIN

The studied Grt-Hbl vein (~ 1 cm-thick) consists of garnet, hornblende, biotite, plagioclase and quartz. It discordantly cuts the gneissose structure of the host (or the wall rock) Grt-Opx-Hbl gneiss (Figs. 2a and 2b). The Grt-Hbl vein is orthopyroxene-free (Fig. 2e). In the host gneiss, orthopyroxene is present in addition to garnet, hornblende, biotite, and plagioclase with rare quartz (Fig. 2f). This sample also contains accessory minerals of zircon, sulfide, ilmenite, iron oxide, and secondary Fe-hydroxide. Garnet is slightly zoned and has almandine-rich compositions both in the vein ($Alm_{57-62}Prp_{19-25}Grs_{15-19}Sps_{2-3}$; X_{Mg} = 0.24-0.30) and away from the vein ($Alm_{58-63}Prp_{20-24}Grs_{14-18}Sps_{2-3}$; X_{Mg} = 0.24-0.28). Calcium-rich domains in garnet become dominant with distance from the vein (Fig. 2c). Hornblende and biotite compositions at the vein center are 2.0 wt% Cl and X_{Mg} = 0.49, and 1.1 wt% Cl and X_{Mg} = 0.61, respectively. Plagioclase is andesine to labradorite and is chemically zoned (An_{45-69}). Sodium-rich rim of plagioclase gets thinner with distance from the vein (Fig. 2d). The mineral assemblage in the vein is typical of upper amphibolite facies *P-T* conditions.

With distance from the Grt-Hbl vein center, the Cl concentration of hornblende and biotite decreases and becomes constant at ~ 1.6 cm away (Fig. 2g). The Pb concentrations of hornblende, biotite and plagioclase decrease as well and become constant at ~ 3.6 cm. Figure 2g shows decreasing Cl and Pb concentrations in hornblende. These observations imply that the Grt-Hbl vein formation altered wall rock mineral compositions up to ~ 3.6 cm from the vein center.

In situ Zr analysis of minerals and whole-rock Zr concentration

In situ LA-ICPMS analysis of garnet, hornblende, orthopyroxene, biotite, plagioclase and apatite was performed to determine their Zr concentration (Table 1). In measuring the Zr concentration of garnet, geometric cores and rims were analyzed over a distance from the vein center, in order to evaluate the chemical zoning in Zr. As a result, garnet showed almost constant Zr concentration (~ 3 ppm) irrespective of the location in the grain and of the distance from the vein (Fig. 2g). Although the Cl concentration of hornblende decreases away from the vein, major element zoning within each hornblende grain was not observed. The Zr concentration of hornblende is almost constant (~ 26 ppm), irrespective of the location in the grain and of the distance from the vein (Fig. 2g). The Zr concentration of orthopyroxene, biotite, plagioclase and apatite present in the matrix as well as those included in garnet and orthopyroxene were low, and not correlated with the location in the grain or the distance from the vein (Table 1).

Table 1. Zirconium concentration in major and accessory minerals* and slices 1-4**

Mineral	Zr (ppm)
Grt	2.8 ± 1.3 (n = 19, 2σ)
Opx	0.8 ± 0.2 (n = 13, 2σ)
Hbl	26.3 ± 2.9 (n = 26, 2σ)
Bt	0.8 ± 0.6 (n = 14, 2σ)
Pl	b.d.
Ap	b.d.
Whole-rock analysis	**Zr (ppm)**
Slice 1 (Grt-Hbl vein)	45.6
Slice 2	53.2
Slice 3	55.1
Slice 4	57.6

* Determined by LA-ICPMS.
** Determined by ICPMS.
Grt, garnet; Opx, orthopyroxene; Hbl, hornblende; Bt, biotite; Pl, plagioclase; Ap, apatite.
b.d., below detection limit.

Slices of the studied sample (1cm thick) were prepared parallel to the Grt-Hbl vein, and whole-rock Zr concentrations of each slice were determined by ICPMS analysis (Table 1). The slices prepared included the Grt-Hbl vein itself (−0.5-0.5 cm; slice 1) and three slices of the wall rock with distance from the vein center being 0.5-1.5 cm (slice 2), 1.5-2.5 cm (slice 3) and 2.5-3.5 cm (slice 4), respectively. Modal amounts of minerals in each slice were also determined using X-ray elemental mapping and electron microscope observation. The results are summarized in Table 2.

In situ LA-ICPMS U-Pb zircon dating and REE analysis

Zircon is included in garnet, orthopyroxene, hornblende, plagioclase and biotite, and is also present in the matrix. Zircon is commonly rounded- to oval-shaped and ~ 20-50 μm in diameter (Fig. 3). Zircon grains share similar microstructural features irrespective of their mode of occurrence and distance from the vein center (Fig. 3). Zircon zoning can be described as follows based on U concentrations and Th/U ratios.

Core: U content < 100 ppm and Th/U ratio = 0.19-0.99.

Table 2. Modal amount of minerals*

Mineral	Slice 1 (Grt-Hbl vein)	Slice 2	Slice 3	Slice 4
Grt	27.7	6.4	8.2	8.1
Opx	2.9	10.8	9.1	12.1
Hbl	22.3	8.0	4.3	5.0
Bt	9.2	18.1	21.4	17.6
Pl	34.1	56.2	56.4	55.8
Qtz	1.7	0.2	0.2	0.3
Ap	2.2	0.4	0.5	1.1
Zrn	0.01	0.01	0.01	0.01
Total (vol%)	100.0	100.0	100.0	100.0

* Obtained from the X-ray elemental mapping and electron microprobe observation.
Qtz, quartz; Zrn, zircon; Other abbreviations are the same as Table 1.

Mantle: U content = 141–306 ppm and Th/U ratio = 0.62–0.99.
Rim: U content = 140–421 ppm and Th/U ratio = 0.43–0.59.

Every zircon grain preserves cores which can be recognized as bright-CL domain (Fig. 3). Mantles and rims are characterized by darker-CL domains than the cores (Fig. 3). Mantles tend to have higher Th/U ratio than the rims. Mantle-rim boundaries are more ambiguous than core-mantle boundaries in CL images. Some zircon grains show very thin mantles or rims, or lack one of them (Fig. 3). No inclusions were seen in the zircon grains studied.

The U-Pb zircon ages and REE concentrations of zircon were determined in order to evaluate the presence or absence of zircon resorption as a function of distance from the vein (Figs. 3, 4, and Table 3). The U-Pb ages with better than 95–105% concordance (where concordance = ($^{206}Pb/^{238}U$ age)*100/($^{207}Pb/^{235}U$ age)) are interpreted as being meaningful concordant ages in this study. Two cores gave $^{206}Pb/^{238}U$ ages of 1175 ± 58 Ma (U = 10 ppm; Th/U = 0.36) and 685 ± 34 Ma (U = 19 ppm; Th/U = 0.25). The mantles (n = 4) gave $^{206}Pb/^{238}U$ ages of 658–630 Ma. The weighted mean $^{206}Pb/^{238}U$ age of the rims (n = 8) is 617 ± 9 Ma (Fig. 4b). Mantles and rims have similar REE concentrations and share the same positively-sloping MREE-HREE pattern with Yb/Dy = 4.7 ± 0.9 (2σ) irrespective of a distance from the Grt-Hbl vein (Fig. 5a and Table 4). Mantles and rims commonly show positive Ce and negative Eu anomalies in chondrite-normalized REE patterns (Fig. 5a). Three core analyses showed different REE patterns from mantles and rims, showing steep and positively-sloping HREE-enriched patterns with Yb/Dy = 24 ± 0.3 (2σ) without a positive Ce anomaly (Fig. 5a). A core with similar REE patterns as mantles and rims also exists (Fig. 5a). As shown in Figures 3, 5b, 5c, and Table 4, no correlation between rim REE patterns, ages, and distance from the vein was detected.

DISCUSSION

Host minerals of Zr

Using the Zr concentrations of minerals and the modal amount of minerals in rock slices 1–4 prepared parallel to the Grt-Hbl vein, the contribution of each mineral to the whole-rock Zr concentration is estimated (Fig. 6, Tables 1, and 2). Garnet and hornblende account for ~ 16% of the whole-rock Zr in the vein itself and the rest of Zr resides in zircon. In the wall rock, 3–5% of the whole-rock Zr resides in garnet and hornblende, and most of the whole-rock Zr is stored in zircon (Fig. 6). Therefore, Zr in this sample mostly resides in zircon irrespective of the distance from the vein (Fig. 6). Since this kind of calculation often accompanies a ~ ± 20% error (e.g., Scambelluri et al., 2006; Marocchi et al., 2010; Xiong et al., 2014), our results are acceptable. Our results for the host mineral of Zr are consistent with Fraser et al. (1997), who studied mafic granulites from the Lützow-Holm Complex, East Antarctica. Hermann (2002) showed that more than 90% of whole-rock Zr is contained in zircon in eclogites from Dora-Maira massif, Western Alps. The present study also confirmed that zircon is the most important sink mineral of Zr in the mafic gneiss collected from the granulite terrane.

Zircon included in the minerals affected by the Grt-Hbl vein formation

The Ca-poor domains of garnet are abundant near the vein (Fig. 2c), suggesting that these domains recrystallized under the effect of Cl-rich fluid or melt when the Grt-Hbl vein was formed. Development of Na-richer plagioclase rims near the vein (Fig. 2d) also suggests that this part of the plagioclase, at least, is affected by the Cl-rich fluid or melt infiltration. Therefore, zircon grains presently included in Ca-poor domains of garnet and Na-richer plagioclase rims could have been the matrix phase during the Cl-rich fluid or melt infiltration, and entrapped in the garnet or plagioclase when the Grt-Hbl vein was formed. Thus, zircon included in these domains can be regarded similarly as zircon in the matrix (Figs. 3 and 5). Zircon grains marked by ‘g’ and ‘p’ in Figures 5b and 5c represent such grains.

Evaluation of Zr as an immobile element

In order to evaluate the appropriateness of Zr as an im-

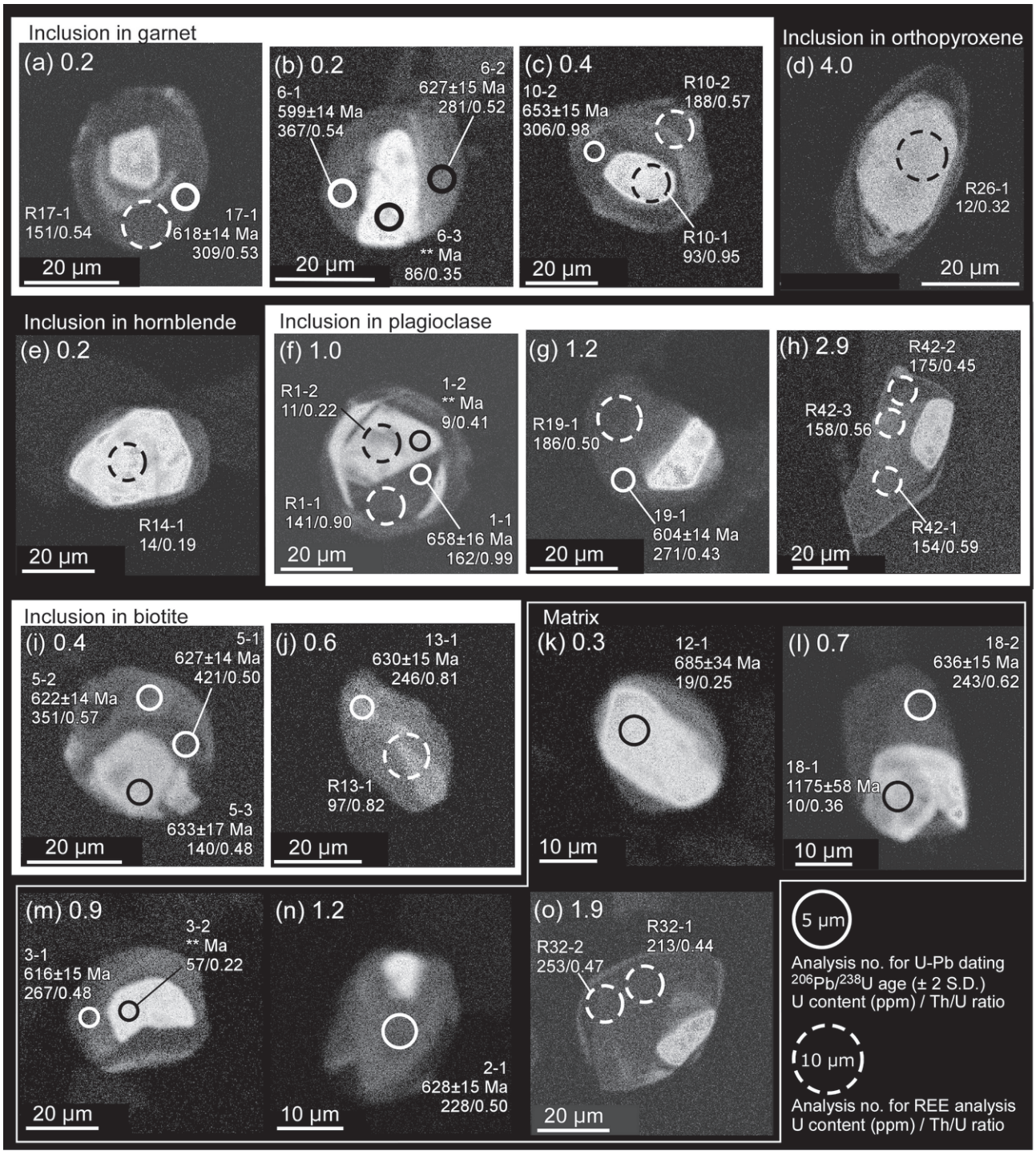

Figure 3. The CL images of zircon with analytical results. Numbers next to alphabets in parentheses represent the distance from the Grt-Hbl vein center (cm) where each zircon grain occurs. Circles represent pits for LA-ICPMS U-Pb dating (5 μm in diameter). From the top to the bottom, numbers next to the circle represent analysis number, $^{206}Pb/^{238}U$ ages ± 2 S.D. error (Ma), U concentration (ppm) and Th/U ratio. '*' represents concordance for the analysis point is out of 95-105%. Dotted circles represent pits for LA-ICPMS REE analysis (10 μm in diameter). From the top to the bottom, numbers next to the dotted circle are analysis number, U concentration (ppm) and Th/U ratio. (a)-(c) Zircon included in garnet. (d) Zircon included in orthopyroxene. (e) Zircon included in hornblende. (f)-(h) Zircon included in plagioclase. (i)-(j) Zircon included in biotite. (k)-(o) Zircon present in the matrix.

mobile element, it is necessary to investigate whether Zr was added or lost during the Grt-Hbl vein formation. The continuous gneissose structure from the wall rock to the vicinity of the vein center (Fig. 2e) suggests that most of

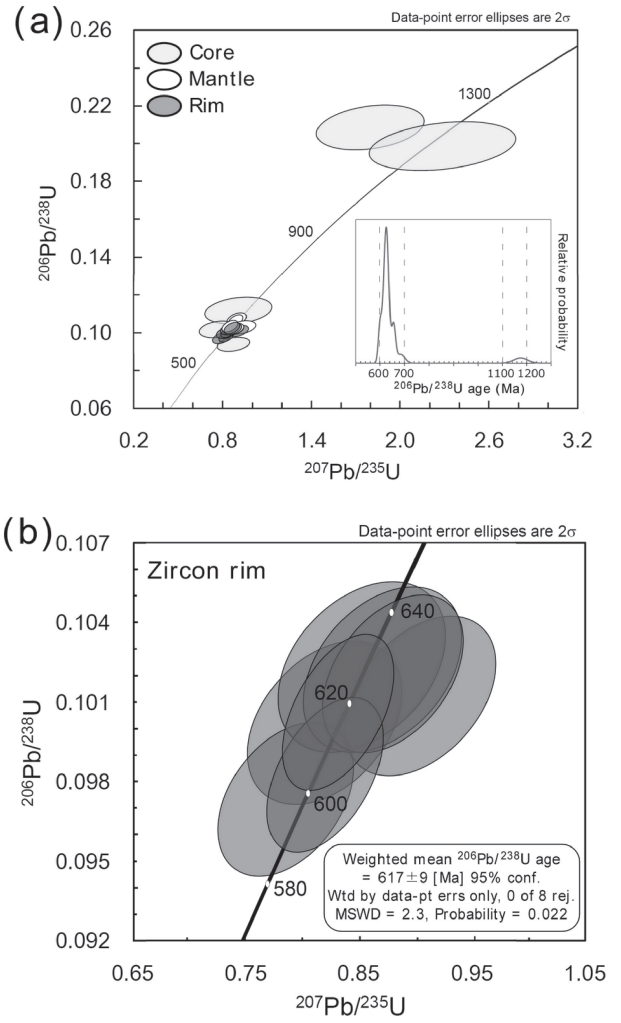

Figure 4. The results of LA-ICPMS U-Pb dating of zircon constructed using Isoplot v.4.13 (Ludwig, 2008). (a) U-Pb concordia plot for all zircon domains and a relative probability diagram for analysis points with 95-105% concordance. (b) U-Pb concordia plot for rims of zircon.

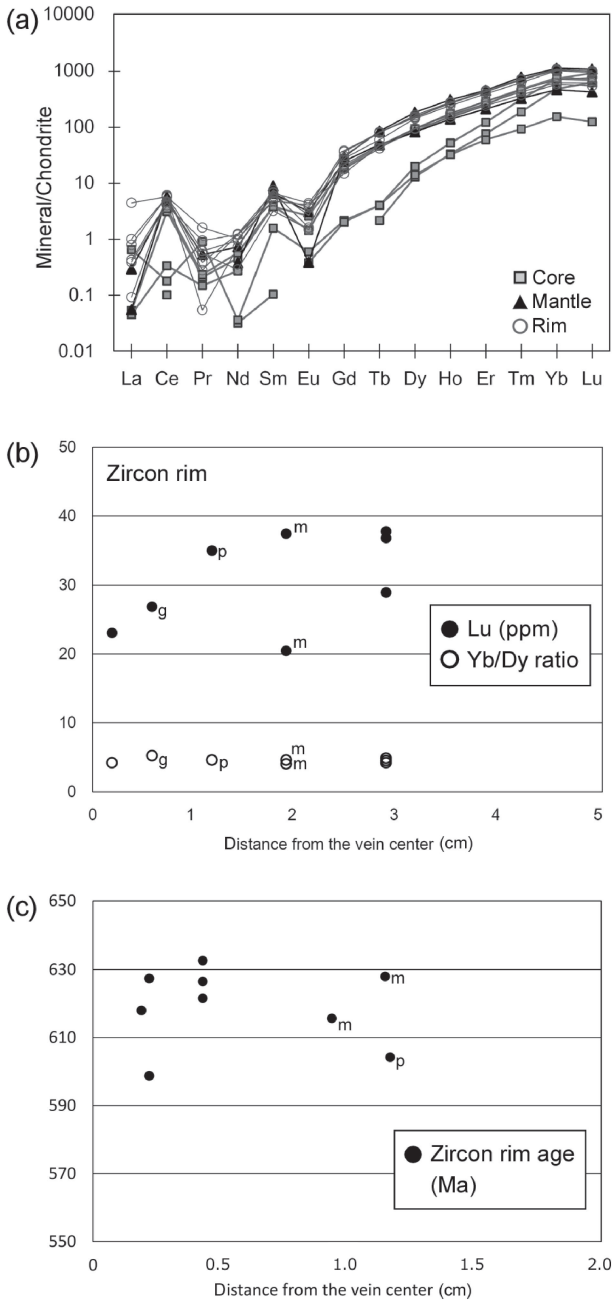

Figure 5. (a) Chondrite-normalized REE patterns of zircon. Zircon rims show similar REE pattern. The REE patterns of zircon cores vary depending on the analysis points. Some cores and mantles show similar REE patterns to the rims. (b) Lutetium concentrations and Yb/Dy ratios of zircon rims with distance from the vein center. REE compositions of zircon rims are constant with distance from the vein. (c) $^{206}Pb/^{238}U$ ages of zircon rim with distance from the vein center. The rim ages are constant with distance from the vein. (b), (c) 'g': zircon included in Ca-poor garnet domain, 'p': zircon included in Na-richer plagioclase rim, 'm': matrix zircon.

the Grt-Hbl vein originated from the wall rock gneiss. However, the modal composition of the minerals in the vein itself is significantly different from that of the wall rock. Therefore, it is highly possible that at least part of the vein was not formed from the wall rock. It is also possible that volume change occurred during the vein formation. On the other hand, the modal amounts of constituent minerals of the wall rock are almost constant irrespective of the distance from the vein. Therefore, it would be better to evaluate the vein itself and the wall rock separately.

First, the wall rock parts (0.5-3.5 cm away from the vein center) are discussed. Whole-rock Zr concentrations are almost constant in the wall rock (Table 1). Both modal amounts and Zr concentrations of garnet and hornblende are also constant irrespective of the distance from the vein (Fig. 2g). These observations imply that Zr addition from the Grt-Hbl vein into the wall rock or Zr loss

Table 3. Summary of the results of LA-ICPMS U-Pb zircon dating

Analysis number		Distance from the vein center (cm)	$^{207}Pb/^{235}U$	2σ	$^{206}Pb/^{238}U$	2σ	r	$^{207}Pb/^{206}Pb$	2σ
02C 2-1	Rim	1.2	0.8523	0.0596	0.1023	0.0026	0.367	0.06042	0.00393
02C 12-1	Core	0.3	0.9026	0.1833	0.1121	0.0058	0.255	0.05841	0.01147
02C 3-1	Rim	0.9	0.8199	0.0549	0.1002	0.0025	0.376	0.05934	0.00368
02C 3-2	Core	0.9	0.7623	0.0994	0.1020	0.0036	0.273	0.05418	0.00679
02C 18-1	Core	0.7	2.2830	0.4050	0.2000	0.0107	0.302	0.08281	0.01401
02C 6-1	Rim	0.2	0.7862	0.0481	0.0973	0.0024	0.397	0.05858	0.00329
02C 6-2	Rim	0.2	0.8704	0.0562	0.1022	0.0025	0.386	0.06175	0.00368
02C 6-3	Core	0.2	0.8679	0.0895	0.0941	0.0030	0.312	0.06688	0.00655
02C 5-1	Rim	0.4	0.8794	0.0500	0.1021	0.0024	0.419	0.06249	0.00323
02C 5-2	Rim	0.4	0.9031	0.0538	0.1012	0.0025	0.408	0.06471	0.00352
02C 5-3	Rim	0.4	0.9254	0.0758	0.1031	0.0029	0.342	0.06509	0.00501
02C 1-1	Mantle	1.0	0.8903	0.0538	0.1075	0.0027	0.424	0.06008	0.00329
02C 1-2	Core	1.0	1.7940	0.2983	0.2100	0.0098	0.281	0.06196	0.00989
02C 13-1	Mantle	0.6	0.8589	0.0442	0.1027	0.0025	0.475	0.06063	0.00275
02C 10-1	Mantle	0.4	0.8829	0.0412	0.1067	0.0025	0.511	0.06003	0.00241
02C 19-1	Rim	1.2	0.8203	0.0414	0.0983	0.0024	0.482	0.06055	0.00268
02C 18-2	Mantle	0.7	0.8451	0.0440	0.1038	0.0025	0.470	0.05908	0.00271
02C 17-1	Rim	0.2	0.8317	0.0396	0.1006	0.0024	0.503	0.05995	0.00247

Analysis number		$^{206}Pb/^{238}U$ age (Ma)	2σ	$^{207}Pb/^{235}U$ age (Ma)	2σ	$^{207}Pb/^{206}Pb$ age (Ma)	2σ	Concordance (%)	U (ppm)	2σ	Th (ppm)	2σ
02C 2-1	Rim	628	15	626	33	619	147	100	228	29	116	14
02C 12-1	Core	685	34	653	103	545	499	105	19	2	5	1
02C 3-1	Rim	616	15	608	31	580	141	101	267	34	130	16
02C 3-2	Core	626	21	575	59	378	310	109	57	7	13	2
02C 18-1	Core	1175	58	1207	134	1265	372	97	10	1	4	0
02C 6-1	Rim	599	14	589	28	552	127	102	367	47	201	24
02C 6-2	Rim	627	15	636	31	666	133	99	281	36	149	18
02C 6-3	Core	580	18	634	50	834	219	91	86	11	31	4
02C 5-1	Rim	626	14	641	27	691	114	98	421	54	215	26
02C 5-2	Rim	622	14	653	29	765	119	95	351	45	201	24
02C 5-3	Rim	633	17	665	41	777	171	95	140	18	68	8
02C 1-1	Mantle	658	16	647	29	607	123	102	162	47	163	33
02C 1-2	Core	1229	53	1043	115	673	384	118	9	3	4	1
02C 13-1	Mantle	630	15	630	24	626	101	100	246	71	203	41
02C 10-1	Mantle	653	15	643	22	605	89	102	306	89	306	61
02C 19-1	Rim	604	14	608	23	623	98	99	271	79	119	24
02C 18-2	Mantle	636	15	622	24	570	103	102	243	70	154	31
02C 17-1	Rim	618	14	615	22	602	92	101	309	90	166	33

out of the wall rock into the vein did not occur during the vein formation. Rims of zircon present in the wall rock show constant Th/U ratios, REE concentrations, REE patterns and U-Pb ages irrespective of a distance from the vein (Figs. 3-5). The grain size of zircon in the wall rock is also constant. Zircon rims did not give younger U-Pb ages than the timing of granulite facies metamorphism reported by previous studies in the study area (e.g., Adachi et al., 2013b). Moreover, there are no microstructures in zircon implying resorption and/or overgrowth (Fig. 3), and re-equilibrium textures of zircon formed in aqueous fluids or melts as reported in Geisler et al. (2007) are also not found. These observations suggest that the zircon grains in the wall rock were not significantly affected, both chemically and microstructurally, by the Grt-Hbl vein formation. Zirconium in other host minerals (garnet and hornblende) did not move significantly because the Zr concentrations and modal amounts of these minerals are constant in the wall rock (Figs. 2 and 6). Therefore, Zr would be described as immobile in the wall rock during the Grt-Hbl vein formation.

Next, behavior of zircon and Zr in the vein itself is discussed. More than ~ 85% of the whole-rock Zr in the vein is hosted in zircon. There is no significant difference

Table 3. (Continued)

Analysis number		Th/U	2σ	Pb (ppm)	2σ
02C 2-1	Rim	0.50	0.02	25	3
02C 12-1	Core	0.25	0.01	2	0
02C 3-1	Rim	0.48	0.02	29	4
02C 3-2	Core	0.22	0.01	6	1
02C 18-1	Core	0.36	0.02	2	0
02C 6-1	Rim	0.54	0.02	39	5
02C 6-2	Rim	0.52	0.02	31	4
02C 6-3	Core	0.35	0.01	9	1
02C 5-1	Rim	0.50	0.02	47	6
02C 5-2	Rim	0.57	0.02	39	5
02C 5-3	Rim	0.48	0.02	16	2
02C 1-1	Mantle	0.99	0.10	20	6
02C 1-2	Core	0.41	0.04	2	1
02C 13-1	Mantle	0.81	0.08	29	8
02C 10-1	Mantle	0.98	0.10	39	11
02C 19-1	Rim	0.43	0.04	28	8
02C 18-2	Mantle	0.62	0.06	28	8
02C 17-1	Rim	0.53	0.05	33	9

in grain size and microstructure between zircon in the Grt-Hbl vein and in the wall rock (Fig. 3). The zircon rims in the vein show similar ages, Th/U ratios, REE concentrations and REE patterns to zircon rims in the wall rock (Figs. 3-5). Therefore, zircon in the vein was also not significantly resorbed and overgrown during the Grt-Hbl vein formation.

On the other hand, whole-rock Zr concentration in the vein is slightly lower than that in the wall rock (Table 1). In addition to this difference, garnet and hornblende host ~ 15% of the whole-rock Zr in the vein, and this percentage is higher than in the wall rock (Fig. 6 and Table 1). There can be several possible interpretations to explain these observations. The first interpretation is to consider the closed system behavior of Zr. The whole-rock Zr concentration in the vein decreased because of a volume increase in the vein itself and that Zr addition/loss did not occur, while minor redistribution of Zr between zircon and other minerals took place. In this case, Zr in the vein can be dealt as immobile.

Addition of low Zr content material to the vein, or removal of Zr-bearing material from the vein can also account for the observation above, and this corresponds to open system behavior of Zr in the vein. In both cases, Zr can be regarded as a mobile element in the vein, and the estimated Zr removal from the vein may reach up to ~ 10% (Table 1) in the present case.

Zirconium has been assumed as being an immobile element during dehydration reactions such as at the transition from the blueschist facies to the eclogite facies (e.g., Gao et al., 2007). However, it is reported that zircon, the most important sink mineral of Zr, might be altered by Cl-bearing fluid under high-T metamorphism (Dunkley, 2010). Detailed analysis of Zr-bearing minerals in this study made it clear that zircon is not altered even during the Grt-Hbl vein formation potentially caused by the Cl-rich fluid or melt infiltration under up-

Table 4. Rare earth element concentrations of zircon determined by LA-ICPMS

Analysis number	121002C R17-1	121002C R14-1	121002C R10-1	121002C R10-2	121002C R13-1	121002C R1-1	121002C R1-2	121002C R19-1	121002C R32-1	121002C R32-2
	Rim	Core	Core	Mantle	Rim	Mantle	Core	Rim	Rim	Rim
Distance from the vein center (cm)	0.2	0.2	0.4	0.4	0.6	1.0	1.0	1.2	1.9	1.9
Y	412	167	378	729	449	336	101	613	368	670
La	0.1	0.2	0.0	0.0	b.d.	0.1	b.d.	0.0	0.2	b.d.
Ce	3.8	0.2	2.9	5.5	3.4	4.6	0.1	5.4	4.4	5.8
Pr	0.1	0.1	0.0	b.d.	0.0	0.1	b.d.	0.1	0.1	0.0
Nd	0.8	0.0	0.3	0.3	0.4	0.5	0.0	0.9	0.2	0.5
Sm	1.1	0.4	0.9	2.0	0.9	1.5	0.0	1.6	0.7	1.5
Eu	0.3	0.1	0.1	0.0	0.2	0.3	0.0	0.1	0.1	0.4
Gd	6.4	0.7	5.5	9.0	5.9	7.4	b.d.	8.4	5.3	9.3
Tb	2.7	0.2	2.6	4.8	2.6	2.8	0.1	3.4	2.4	4.7
Dy	35.7	7.5	31.4	69.0	35.1	30.7	4.8	53.6	34.9	57.5
Ho	13.8	4.4	13.0	25.8	14.5	11.7	2.8	20.3	12.4	22.8
Er	64.5	29.8	61.2	111	70.5	51.8	18.8	96.0	59.2	110
Tm	15.0	11.0	16.6	27.4	16.5	11.4	6.6	21.8	13.1	25.1
Yb	151	178	177	275	184	114	117	247	141	266
Lu	23.0	34.4	25.6	40.7	26.9	15.9	23.3	35.0	20.4	37.4
Hf	6759	9976	8776	10423	5710	8154	8823	9252	7496	9646
Th	81.1	2.8	88.3	107	79.7	127	2.3	93.2	94.5	119
U	151	14.2	93.3	188	97.4	141	10.7	186	213	253

Table 4. (Continued)

Analysis number	121002C R42-1	121002C R42-2	121002C R42-3	121002C R26-1
	Rim	Rim	Rim	Core
Distance from the vein center (cm)	2.9	2.9	2.9	4.0
Y	666	450	646	107
La	0.3	1.6	0.4	0.0
Ce	5.5	5.4	5.5	0.3
Pr	0.1	0.2	0.0	0.0
Nd	0.7	0.7	0.8	0.2
Sm	1.7	1.1	1.3	b.d.
Eu	0.2	0.4	0.3	0.0
Gd	10.9	4.5	11.4	0.6
Tb	4.5	2.7	4.6	0.2
Dy	61.0	35.3	56.0	5.3
Ho	23.3	14.9	22.2	2.7
Er	104	70.7	104	14.6
Tm	24.7	16.1	24.3	3.3
Yb	257	172	254	37.6
Lu	36.8	28.9	37.7	4.7
Hf	9457	7833	9463	11101
Th	90.7	78.8	88.8	4.0
U	154	175	158	12.4

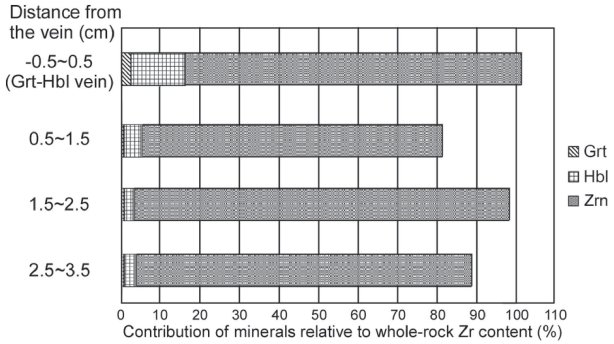

Figure 6. Zirconium distribution among the minerals in sample TK2009121002C, shown as a function of the distance from the Grt-Hbl vein. The whole rock Zr contents of each zones were obtained from the whole-rock Zr analysis by ICPMS, which was compared with the total Zr contents in each mineral calculated from the modal amount of minerals and Zr contents of each mineral determined by LA-ICPMS analyses (Tables 1 and 2). Garnet, hornblende, and zircon are shown in this figure, because they are recognized as host mineral of Zr. Zircon is the main host mineral of Zr irrespective of the distance from the vein. Although ilmenite could be an additional carrier of Zr (Degenhardt, 1957), it is not considered here because of its low modal amount and low Zr concentration.

per amphibolite facies condition, and Zr can be dealt as immobile in the wall rock during the Grt-Hbl vein formation. Therefore, in most of the rocks in which zircon is the major host of Zr, as attempted in this study, observing the presence or absence of zircon resorption/recrystallization through combined microstructural and chemical approaches will help evaluate whether Zr could become an appropriate 'immobile element' or not.

ACKNOWLEDGMENTS

We would like to thank Dr. Y. Saitoh and an anonymous reviewer for constructive reviews and Prof. T. Tsunogae for editorial efforts. Thanks are also due to members of the JARE geology group for their fruitful discussions. This study was financially supported by Grant-in-Aid for JSPS Fellows (No. 25·715) to F. Higashino, the Grant-in-Aid for Young Scientist (B) (No. 23740391) and Grant-in-Aid for Scientific Research (C) (No. 26400513) to T. Kawakami, and Grant-in-Aid for Scientific Research (A) (No. 22244067) to T. Hirajima.

SUPPLEMENTARY MATERIALS

Tables S1 and S2 are available online from http://doi.org/10.2465/jmps.150220.

REFERENCES

Adachi, T., Hokada, T., Osanai, Y., Nakano, N., Baba, S. and Toyoshima, T. (2013a) Contrasting metamorphic records and their implications for tectonic process in the central Sør Rondane Mountains, eastern Dronning Maud Land, East Antarctica. Geological Society London, 383, 113-133.

Adachi, T., Osanai, Y., Hokada, T., Nakano, N., Baba, S. and Toyoshima, T. (2013b) Timing of metamorphism in the central Sør Rondane Mountains, eastern Dronning Maud Land, East Antarctica: Constrains from SHRIMP zircon and EPMA monazite dating. Precambrian Research, 234, 136-160.

Ague, J. (2003) Fluid infiltration and transport of major, minor, and trace elements during regional metamorphism of carbonate rocks, Wepawaug Schist, Connecticut, USA. American Journal of Science, 303, 753-816.

Ague, J.J. and Van Haren, L.M. (1996) Assessing metamorphic mass and volume changes using the bootstrap, with application to deep crustal hydrothermal alteration of marble. Economic Geology, 91, 1169-1182.

Asami, M., Osanai, Y., Shiraishi, K. and Makimoto, H. (1992) Metamorphic evolution of the Sør Rondane Mountains, East Antarctica. In Recent Progress in Antarctic Earth Science (Yoshida, Y., Kaminuma, K. and Shiraishi, K. Eds.). Terra Scientific Publishing Company, Tokyo, 7-15.

Ayers, J.C. and Watson, E.B. (1991) Solubility of apatite, monazite, zircon, and rutile in supercritical aqueous fluids with implications for subduction zone geochemistry. Philosophical Transactions of the Royal Society of London Series A, 335, 365-375.

Degenhardt, H. (1957) Untersuchungen zur geochemischen Verteilung des Zirkoniums in der Lithosphäre. Geochimica et Cosmochimica Acta, 11, 279-300 (in German with English abstract).

Dill, H.G. (2010) The "chessboard" classification scheme of mineral deposits: Mineralogy and geology from aluminum to zir-

conium. Earth-Science Reviews, 100, 1-420.
Dunkley, D.J. (2010) Textural diagnosis of zircon re-equilibration by fluids and melts during high-*T* metamorphism. Geochimica et Cosmochimica Acta, 74, A252.
Fraser, G., Ellis, D. and Eggins, S. (1997) Zirconium abundance in granulite-facies minerals, with implications for zircon geochronology in high-grade rocks. Geology, 25, 607-610.
Gao, J., John, T., Klemd, R. and Xiong, X. (2007) Mobilization of Ti-Nb-Ta during subduction: Evidence from rutile-bearing dehydration segregations and veins hosted in eclogite, Tianshan, NW China. Geochimica et Cosmochimica Acta, 71, 4974-4996.
Geisler, T., Schaltegger, U. and Tomaschek, F. (2007) Re-equilibration of zircon in aqueous fluids and melts. Elements, 3, 43-50.
Grant, J.A. (1986) The isocon diagram — a simple solution to Gresens' equation for metasomatic alteration. Economic Geology, 81, 1976-1982.
Grantham, G.H., Macey, P.H., Horie, K., Kawakami, T., Ishikawa, M., Satish-Kumar, M., Tsuchiya, N., Graser, P. and Azevedo, S. (2013) Comparison of the metamorphic history of the Monapo Complex, northern Mozambique and Balchenfjella and Austhamaren areas Sør Rondane, Antarctica: Implications for the Kuunga Orogeny and the amalgamation of N and S. Gondwana. Precambrian Research, 234, 85-135.
Harlov, D.E. and Dunkley, D.J. (2011) Experimental high-grade alteration of zircon using alkali- and Ca-bearing solutions. Mineralogical Magazine, 77, 980.
Hermann, J. (2002) Allanite: thorium and light rare earth element carrier in subducted crust. Chemical geology, 192, 289-306.
Higashino, F., Kawakami, T., Satish-Kumar, M., Ishikawa, M. and Grantham, G.H. (2013a) Multi-stage Cl-rich fluid activity and behavior of REE-bearing minerals in a Neoproterozoic granulite terrane. Mineralogical Magazine, 77, 1298.
Higashino, F., Kawakami, T., Satish-Kumar, M., Ishikawa, M., Maki, K., Tsuchiya, N., Grantham, G.H. and Hirata, T. (2013b) Chlorine-rich fluid or melt activity during granulite facies metamorphism in the Late Proterozoic to Cambrian continental collision zone — An example from the Sør Rondane Mountains, East Antarctica. Precambrian Research, 234, 229-246.
Hirata, T. and Kon, Y. (2008) Evaluation of analytical capability of NIR femtosecond laser ablation-inductively coupled plasma mass spectrometry. Analytical Sciences, 24, 345-353.
Hirata, T. and Nesbitt, R.W. (1995) U-Pb Isotope Geochronology of Zircon: Evaluation of the Laser Probe-Inductively Coupled Plasma Mass Spectrometry Technique. Geochimica et Cosmochimica Acta. 59, 2491-2500.
Iizuka, T. and Hirata, T. (2004) Simultaneous determinations of U-Pb age and REE abundances of zircon crystals using ArF Excimer laser ablation-inductively coupled plasma-mass spectrometry equipped with a Chicane ion lens system. Geochemical Journal, 38, 229-241.
Ishikawa, M., Kawakami, T., Satish-Kumar, M., Grantham, G.H., Hokazono, Y., Saso, M. and Tsuchiya, N. (2013) Late Neoproterozoic extensional detachment in eastern Sør Rondane Mountains, East Antarctica: Implications for the collapse of East African Antarctic Orogen. Precambrian Research, 234, 247-256.
Jacobs, J. and Thomas, R.J. (2004) Himalayan-type indenter-escape tectonics model for the southern part of the late Neoproterozoic-early Paleozoic East African-Antarctic orogeny. Geology, 32, 721-724.
Kretz, R. (1983) Symbols for rock-forming minerals. American Mineralogist, 68, 277-279.
Li, Z.L., Chen, H., Yang, S., Tainosho, Y., Shiraishi, K. and Owada, M. (2007) Fluid components in accessory minerals of Pan-African granitoids in the Sør Rondane Mountains, East Antarctica. Journal of Zhejiang University SCIENCE A, 8, 1004-1010.
Ludwig, K.R. (2008) User's Manual for Isoplot 3.70. A geological toolkit for Microsoft Excel. Berkeley Geochronology Center Special Publication No. 4 (revision of August 26, 2008).
Marocchi, M., Hermann, J., Tropper, P., Bargossi, G.M. and Mair, V. (2010) Amphibole and phlogopite in "hybrid" metasomatic bands monitor trace element transfer at the interface between felsic and ultramafic rocks (Eastern Alps, Italy). Lithos, 117, 135-148.
Meert, J. (2003) A synopsis of events related to the assembly of eastern Gondwana. Tectonophysics, 362, 1-40.
Mori, Y., Nishiyama, T. and Yanagi, T. (2007) Chemical mass balance in a reaction zone between serpentinite and metapelites in the Nishisonogi metamorphic rocks, Kyushu, Japan: Implications for devolatilization. Island Arc, 16, 28-39.
Olsen, S.N. and Grant, J.A. (1991) Isocon analysis of migmatization in the Front Range, Colorado, USA. Journal of Metamorphic Geology, 9, 151-164.
Osanai, Y., Nogi, Y., Baba, S., Nakano, N., Adachi, T., Hokada, T., Toyoshima, T., Owada, M., Satish-Kumar, M., Kamei, A. and Kitano, I. (2013) Geologic evolution of the Sør Rondane Mountains, East Antarctica: Collision tectonics proposed based on metamorphic processes and magnetic anomalies. Precambrian Research, 234, 8-29.
Rubin, J.N., Henry, C.D. and Proce, J.G. (1993) The mobility of zirconium and other "immobile" elements during hydrothermal alteration. Chemical Geology, 110, 29-47.
Sakata, S., Hattori, K., Iwano, H., Yokoyama, T.D., Danhara, T. and Hirata, T. (2014) Determination of U-Pb Ages for Young Zircons using Laser Ablation-ICP-Mass Spectrometry Coupled with an Ion Detection Attenuator Device. Geostandards and Geoanalytical Research, 38, 409-420.
Scambelluri, M., Hermann, J., Morten, L. and Rampone, E. (2006) Melt- versus fluid-induced metamorphism in spinel to garnet wedge peridotites (Ulten Zone, Eastern Italian Alps): clues from trace element and Li abundances. Contributions to Mineralogy and Petrology, 151, 372-394.
Shiraishi, K. and Kojima, S. (1987) Basic and intermediate gneisses from the western part of the Sør Rondane Mountains, East Antarctica. Proceedings of the NIPR symposium on Antarctic Geosciences, 1, 129-149.
Shiraishi, K., Asami, M., Ishizuka, H., Kojima, H., Kojima, S., Osanai, Y., Sakiyama, T., Takahashi, Y., Yamazaki, M. and Yoshikura, S. (1991) Geology and metamorphism of the Sør Rondane Mountains, East Antarctica. In Geological Evolution of Antarctica (Thomsom, M.R.A., Crame, J.A. and Thomson, J.W. Eds.). Cambridge University Press, Cambridge, 77-82.
Shiraishi, K., Dunkley, D.J., Hokada, T., Fanning, C.M., Kagami, H. and Hamamoto, T. (2008) Geochronological constrains on the Late Proterozoic to Cambrian crustal evolution of eastern Dronning Maud Land, East Antarctica: a synthesis of SHRIMP U-Pb age and Nd model age data. Geological Society of London, 308, 21-67.
Taylor, R.J.M., Clark, C., Fitzsimons, I.C.W., Santosh, M., Hand, M., Evans, N. and McDonald, B. (2014) Post-peak, fluid-

mediated modification of granulite facies zircon and monazite in the Trivandrum Block, southern India. Contributions to Mineralogy and Petrology, 168, 1–17.

Toyoshima, T., Osanai, Y., Baba, S., Hokada, T., Nakano, N., Adachi, T., Otsubo, M., Ishikawa, M. and Nogi, Y. (2013) Sinistral transpressional and extensional tectonics in Dronning Maud Land, East Antarctica, including the Sør Rondane Mountains. Precambrian Research, 234, 30–46.

Tsuchiya, N., Ishikawa, M., Satish-Kumar, M., Kawakami, T., Kojima, H., Kaiden, H., Miura, H., Suganuma, Y., Abe, M., Sasaki, D., Chiba, M., Okada, Y., Hashizume, F., Grantham, G. and Goreris, S. (2012) Report on geological fieldwork in the Sør Rondane Mountains, Eastern Dronning Maud Land, 2009–2010 (JARE-51). Antarctic Record, 56, 295–379.

Whitbread, M.A. and Moore, C.L. (2004) Two lithogeochemical approaches to the identification of alteration patterns at the Elura Zn–Pb–Ag deposit, Cobar, New South Wales, Australia: use of pearce Element Ratio analysis and Isocon analysis. Geochemistry: Exploration, Environment, Analysis, 4, 129–141.

Xiong, Q., Zheng, J.-P., Griffin, W.L., O'reilly, S.Y. and Pearson, N.J. (2014) Pyroxenite dykes in orogenic peridotite from North Qaidam (NE Tibet, China) track metasomatism and segregation in the mantle wedge. Journal of Petrology, 55, 2347–2376.

Yamasaki, S. (1996) Inductively coupled plasma mass spectrometry. In Mass Spectrometry of Soils (Boutton, T. and Yamasaki, S. Eds.). Marcel Dekker, New York, 459–491.

Yamasaki, S., Takeda, A., Nunohara, K. and Tsuchiya, N. (2013) Red soils derived from limestone contain higher amounts of trace elements than those derived from various other parent materials. Soil Science and Plant Nutrition, 59, 692–699.

Manuscript received February 20, 2015
Manuscript accepted May 11, 2015
Published online July 1, 2015
Manuscript handled by Toshiaki Tsunogae